INSTITUTE OF PHYSICS PUBLISHING NANOTECHNOLOGY
Nanotechnology **18** (2007) 035504 (6pp) doi:10.1088/0957-4484/18/3/035504

Imaging nanoparticle flow using magneto-motive optical Doppler tomography

Jeehyun Kim[1,3], **Junghwan Oh**[2,3], **Thomas E Milner**[2] **and J Stuart Nelson**[1]

[1] Beckman Laser Institute and Medical Clinic, University of California, 1002 Health Sciences Road East, Irvine, CA 92612, USA
[2] Biomedical Engineering Department, University of Texas, Austin, TX 78712, USA

E-mail: jeehk@uci.edu

Received 6 September 2006, in final form 3 November 2006
Published 3 January 2007
Online at stacks.iop.org/Nano/18/035504

Abstract
We introduce a novel approach for imaging solutions of superparamagnetic iron oxide (SPIO) nanoparticles using magneto-motive optical Doppler tomography (MM-ODT). MM-ODT combines an externally applied temporally oscillating high-strength magnetic field with ODT to detect nanoparticles flowing through a microfluidic channel. A solenoid with a cone-shaped ferrite core extensively increased the magnetic field strength ($B_{max} = 1$ T, $\nabla|B|^2 = 220$ T^2 m^{-1}) at the tip of the core and also focused the magnetic field in microfluidic channels containing nanoparticle solutions. Nanoparticle contrast was demonstrated in a microfluidic channel filled with an SPIO solution by imaging the Doppler frequency shift which was observed independently of the nanoparticle flow rate and direction. Results suggest that MM-ODT may be applied to image Doppler shift of SPIO nanoparticles in microfluidic flows with high contrast.

(Some figures in this article are in colour only in the electronic version)

Rapid progress in the nanosciences and requirement to characterize structures and particles has led investigators to utilize several sophisticated imaging modalities including atomic force microscopy (AFM), magnetic force microscopy (MFM) and scanning near-field optical microscopy (SNOM). Most of these techniques utilize a probe that has a nanometre-sized sharp tip to allow imaging of a gas–solid interface with nanometre scale. As a micrometre scale imaging modality, optical coherence tomography (OCT) uses the short temporal coherence properties of broadband light to extract structural information from heterogeneous optically turbid samples such as biological tissue. During the past decade, numerous advancements in OCT have been reported including increased resolution (2–3 μm) [3] and real-time imaging speeds [9]. To date, OCT is not widely utilized in the nanosciences due to relatively poor axial and lateral resolutions. Recently, OCT and ultrasound (US) imaging methods have been demonstrated to image cells and tissues containing paramagnetic iron oxide nanoparticles [7, 6]. These methods, referred to as magneto-motive OCT and US respectively, utilize an externally applied high-strength magnetic field gradient to activate mechanical movement of the nanoparticles. The nanoparticle movement produces a local time-varying mechanical strain field that is detected with OCT or US.

Magnetic nanoparticles are of great interest because of the unique properties of magnetism in nanomaterials and ability to control at a distance without mechanical contact. Magnetic nanoparticles attract significant interest in the applied sciences due to possible technological applications for information storage, magnetic refrigeration, bioprocessing gas sensors and ferrofluids, to name a few. Ferrofluids have numerous potential application/market areas including ferrofluid steppers, gauges and sensors [17, 12]. Monitoring/manipulating of ferrofluidic-based micro-channels is also of interest [4].

Since the ability to characterize fluid flow velocity using OCT was first demonstrated by Wang *et al* [13], several phase

[3] These authors made equal contributions.

resolved [18], real-time [10, 11] optical Doppler tomography (ODT) approaches have been reported. In ODT, the Doppler frequency shift is proportional to the projection of the scattering wavevector $(k_s - k_i)$ on the scatterer's flow direction. When the two directions are perpendicular, the projection is zero and no Doppler shift is observed. Because *a priori* knowledge of the Doppler angle is usually not available, and conventional intensity OCT imaging provides a low contrast image of microfluidic flow, detecting flow in small-diameter microfluidic channels is difficult. In this paper, we demonstrate a novel mechanism to increase contrast in ODT images by using superparamagnetic iron oxide (SPIOs) nanoparticles activated with an externally applied magnetic field. The use of SPIOs as contrast agents for magnetic resonance (MR) imaging of bowel, liver, spleen, lymph nodes, bone marrow, perfusion and angiography [14] has been extensively studied since the early 1990s [2, 15]. The magneto-motive ODT method was reported for detecting red blood cells (RBCs) that are important endogenous contrast agents in the biomedical optics field [5]. However, RBCs are very weakly paramagnetic with a magnetic susceptibility ($\chi \sim 10^{-5}$), whereas SPIOs susceptibility is unity. This means that SPIOs can be actuated with much lower magnetic field intensity.

Herein we present a novel extension of the magneto-motive approach by modulating the Doppler shift to improve magnetic nanoparticle contrast. Contrast in ODT images is enhanced by activating mechanical motion of the nanoparticles with an externally applied high-strength magnetic field gradient. We describe the magneto-motive optical Doppler tomography (MM-ODT) experimental setup and present Doppler images of flowing SPIO nanoparticles under the influence of an externally applied magnetic field gradient.

The material parameter characterizing magnetic materials is the magnetic volume susceptibility, χ, which is dimensionless in SI units and is defined by the equation $\boldsymbol{M} = \chi \boldsymbol{H}$ where $\boldsymbol{M}$ is the magnetization at the point under study and $\boldsymbol{H}$ is the local density of magnetic field strength. A SPIO with $\chi \approx 1$ suspended in solution and placed in a magnetic field gradient experiences forces and torques that tend to position and align it with respect to the field's direction. Magnetic energy, U, of a SPIO nanoparticle in an external magnetic field is given by,

$$U = -\frac{1}{2}\mathbf{m} \cdot \mathbf{B} = -\frac{\Delta\chi V}{2u_0}|\mathbf{B}|^2$$

where $\mathbf{m}$ is the magnetic moment, $\mathbf{B}$ is the magnetic flux density, V is the particle volume, μ_0 is the permeability of free space and $\Delta\chi$ is the difference between susceptibility of the nanoparticle and surrounding solution. Magnetic force acting on SPIO nanoparticles becomes:

$$\mathbf{F} = -\nabla U = \nabla\left(\frac{\Delta\chi V}{2u_0}|\mathbf{B}|^2\right) = \Delta\chi V \nabla\left(\frac{|\mathbf{B}|^2}{2u_0}\right).$$

In our experiments we apply a sinusoidal magnetic flux density that is directed principally along the z direction. Hence, we write $\vec{\mathbf{B}}(x, y, z; t) = \sin(2\pi f_m t)B_z(z)\hat{k}$ and the magnetic force $\mathbf{F_m}$ acting on nanoparticles,

$$\mathbf{F_m} = \frac{\chi_s V_s}{2\mu_0}[1 - \cos(4\pi f_m t)]\mathbf{B}_z(z)\frac{\partial \mathbf{B}_z}{\partial z}$$

where f_m is the modulation frequency of the applied sinusoidal magnetic field.

In addition to the magnetic force, the SPIO nanoparticle experiences a pressure gradient, body, viscous drag forces which combine to produce a dynamic displacement $[z(t)]$ that can be included in the analytic OCT fringe expression [3], I_f,

$$I_f \propto 2\sqrt{I_R I_S}\exp\left[i\left(2\pi f_0 t + \frac{4\pi n \cdot z(t)}{\lambda_0}\right)\right],$$

where I_R and I_S are the back-scattered intensities from reference and sample arms, respectively, f_0 is the fringe carrier frequency, n is the medium refractive index, $z(t)$ is the dynamic nanoparticle displacement and λ_0 is the light source centre wavelength.

A schematic of the MM-ODT apparatus is shown in figure 1. The ODT light source consisted of a superluminescent diode (B&W TEK, DE) centred at 1.3 μm with a bandwidth of 90 nm. Light was coupled into a single-mode optical fibre based interferometer that provided 1 mW of optical power on the microfluid channel containing SPIO solutions. A rapid-scanning optical delay (RSOD) line was used in the reference arm and aligned such that no phase modulation was generated when the group phase delay was scanned at 4 kHz. Phase modulation was generated using an electro-optic waveguide phase modulator that produced a single carrier frequency (1 MHz). To reduce intensity noise from the OCT interference signal, a dual-balanced photodetector was used. A hardware in-phase and quadrature demodulator with high/bandpass filters was constructed to improve imaging speed. Doppler information was calculated with the Kasai autocorrelation velocity estimator [16]. Labview software (National Instruments, Austin, TX) was used to implement the MM-ODT system with a dual processor based multitasking scheme. The maximum frame rate of the system was 16 frames per second for a 400 × 512 pixel sized image. In the sample path of the interferometer, a collimated beam was redirected to the microfluidic channel by two galvanometers and a scanning system that permitted three-dimensional scanning. The probe beam was focused by an objective lens, which yielded a 10 μm diameter spot at the focal point. A 500 μm inner-diameter glass capillary tube was used as a microfluidic channel and placed perpendicularly to the probe beam. SPIO solutions used for flow studies were injected through the tube at a constant flow rate controlled by a dual-syringe pump (Harvard Apparatus 11 Plus, Holliston, MA) with ±0.5% flow rate accuracy.

A solenoid coil (manufacturer: Ledex, part number: 4EF) with a cone-shaped ferrite core at the centre (figure 2) and driven by a current amplifier supplying up to 960 W was placed underneath the sample during MM-ODT imaging. The combination of the core and solenoid, using high power operation, dramatically increased the magnetic field strength ($B_{max} = 1$ T and $\Delta|B|^2 = 220$ T^2 m^{-1}) at the tip of the core and also focused the magnetic force on the targeted samples. The magnetic force applied to the capillary tube was varied by a sinusoidal current to induce SPIO nanoparticle movement. The capillary tube was placed upon a 1 mm thick base plate. The optical access was performed only from one side of the device. The black dotted arrow line at figure 2 represents the light path for M-mode scanning. For B-mode scanning, the

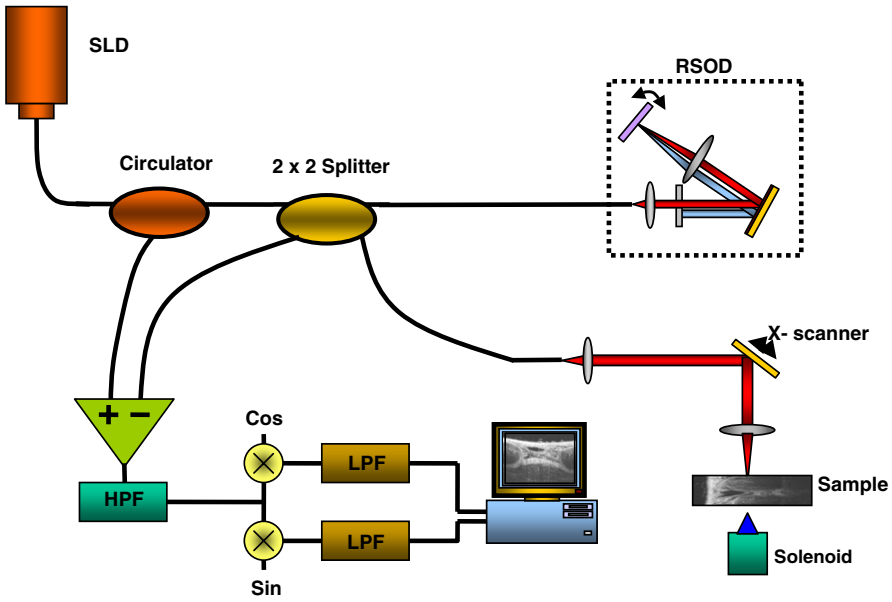

Figure 1. Schematic diagram of the MM-ODT system. SLD: super-luminescent diode, HPF: high pass filter, LPF: low pass filter, RSOD: rapid scanning optical delay line.

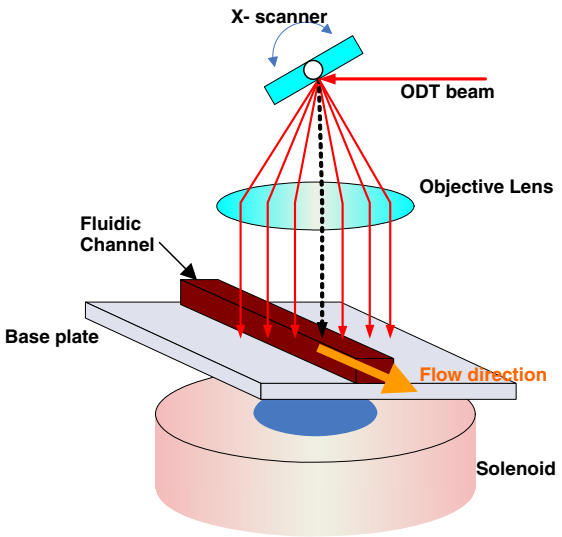

Figure 2. Schematic diagram of the probe beam, flow sample and solenoid.

scanning mirror (figure 2) was driven at 8 Hz, and the solid arrow lines represent the light path.

Nanoparticle solutions were prepared to observe Doppler shifts in a flow channel. Feridex I.V. SPIO nanoparticles with a 5 nm core diameter and dextran coating giving a nominal 100 nm diameter (Advanced Magnetics, Inc.) were used in all experiments. The prepared nanoparticle solution consisted of 50 ml 5% dextrose solution and 1 ml pure Feridex I.V. with a concentration of 0.67×10^{12} iron particles μl^{-1} ($1.12\ \mu g$ iron μl^{-1}) [1].

To demonstrate MM-ODT detection of nanoparticles in solution, we first recorded B-mode OCT/ODT images of a rectangular glass capillary tube filled with a flowing near-zero susceptibility turbid solution without and with an external magnetic field as a control sample. The near-zero susceptibility turbid solution was a mixture of deionized water and 0.5 μm latex microspheres ($\mu_s = 5\ \text{mm}^{-1}$) at a 13 mm s^{-1} flowrate. The magnetic flux density and its frequency were approximately 1 T and 40 Hz, respectively. The field gradient, $\partial B/\partial z$, over 1 mm was 220 kT mm^{-1}. B-mode OCT/ODT images were acquired over a 650 μm $\times$ 650 μm cross section in the microfluidic channel. Figures 3(a) and (b) show B-mode OCT and ODT images without any external magnetic field, whereas figures 3(c) and (d) show B-mode OCT/ODT images with a 40 Hz externally applied magnetic field. No distinguishable Doppler shift is observed in the ODT image with applied magnetic field (figure 3(d)) indicating no interaction between the external magnetic field and turbid solution without nanoparticles.

An SPIO nanoparticle solution was injected through the glass capillary tube by a syringe pump at a constant flow rate. An oscillating Doppler frequency shift resulting from nanoparticle movement could be observed (figure 4) at three flow rates (3, 12, and 30 mm s^{-1}). The angle between the probing beam and the tube was set at 5% so that the Doppler phase shift did not wrap, at the high flow rate (30 mm s^{-1}). In our experiments, the probe beam was first aligned at the centre of the conical ferrite core, and the tube was placed just above the conical tip so that the direction of the field gradient was parallel to the probe beam (along the z direction). M-mode MM-ODT images (figure 4) consisted of 634 $\times$ 400 pixels axially and temporally, respectively, resulting in an image acquisition time of 100 ms. The images were recorded after 5 s following activation of the magnetic field. A Doppler frequency shift of 100 Hz was continuously observed during the magnetic activation. The flow velocity can be quantified as

$$\langle v \rangle = \frac{\lambda_0 f_D}{2n \cos\theta}$$

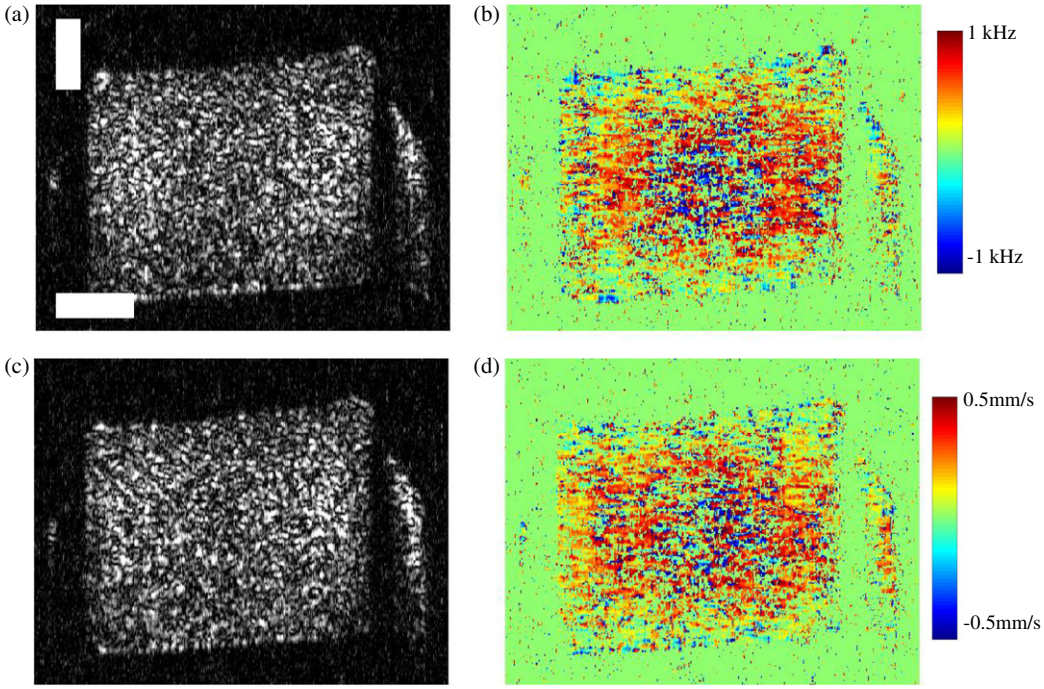

Figure 3. OCT/ODT B-mode images of a stationary low-susceptibility turbid solution without and with an external magnetic field. (a), (b) OCT and ODT B-mode images without an external magnetic field, respectively. (c), (d) OCT and ODT images with a 40 Hz magnetic field, respectively. White vertical and horizontal bars: 200 μm.

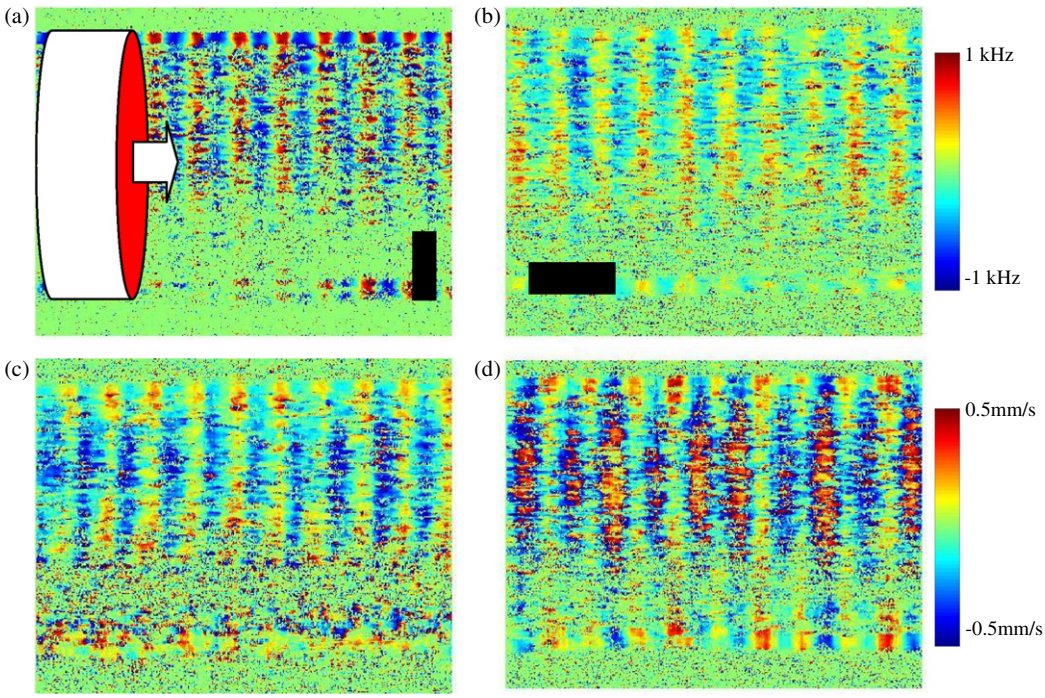

Figure 4. M-mode MM-ODT images of SPIO nanoparticle flow (1.12 μg μl^{-1}) with an externally applied 50 Hz magnetic field. (a)–(d) 0, 3, 12, 30 mm s^{-1}, respectively. Black vertical bar: 200 μm, black horizontal bar: 20 ms.

where λ_0 is the centre wavelength (1.3 μm), f_D is the Doppler frequency, n is the refractive index (1.3), and θ is the angle (5°) between the flow and probe beam direction.

The observed Doppler frequency (100 Hz) was double that of the applied B field (50 Hz) according to the magnetic force (Fm). The cylinder in figures 4 and 6(a) represents the inner wall of the tube and the arrow indicates flow direction. The vertical and horizontal bars indicate 200 μm axially and 20 ms temporally, respectively. B-mode MM-ODT images of a diluted SPIO nanoparticle solution (1.12 μg μl^{-1}) with

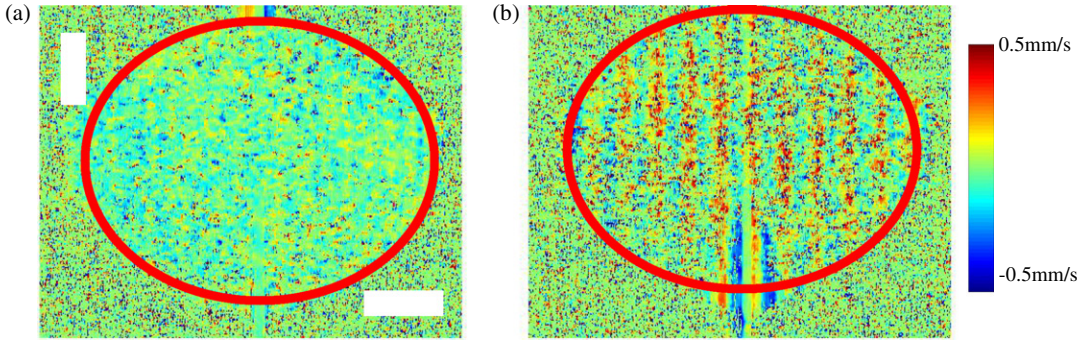

Figure 5. B-mode MM-ODT images of a diluted SPIO nanoparticle (1.12 μg μl^{-1}) with an externally applied 40 Hz magnetic field. (a), (b) ODT B-mode image without and with an external magnetic field, respectively. White vertical and horizontal bars: 200 μm.

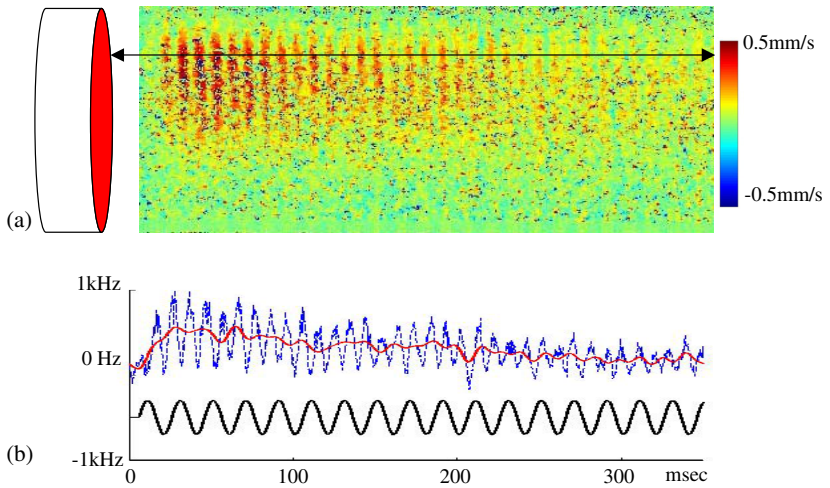

Figure 6. Transient Doppler frequency shift during the first 350 ms of magnetic field application: (a) M-mode MM-ODT image, (b) Doppler frequency shift profile calculated from the arrowed area in (a). Dotted line: average of 20 lines in depth near the arrowed area. Solid line: low pass-filtered signal of the dotted line using an average moving window. Black line: 50 Hz magnetic field signal started at 5 ms.

an externally applied 40 Hz magnetic field are shown in figures 5(a), (b) without and with an external magnetic field, respectively. White vertical and horizontal bars represent a 200 μm length.

To investigate the initial transient response of SPIO nanoparticles to the applied magnetic field, another M-mode MM-ODT image (figure 6) was acquired over 350 ms immediately after the magnetic field was activated. Again, the cylinder in figure 6(a) indicates the inner wall of the tube. Doppler frequency shift profiles (figure 6(b) dotted line) were calculated from the ODT image (figure 6(a)) by averaging 20 lines indicated by the horizontal arrows. The solid line in figure 6(b) was low-pass filtered to remove the 100 Hz component, and the black line indicates the externally applied 50 Hz magnetic field started at 5 ms.

Superparamagnetic nanoparticles under the influence of a strong magnetic field gradient tend to move toward the field source. As the local concentration of nanoparticles increases in response to an external magnetic field, osmotic and elastic recoil forces from the inner tube boundary increase and hinder further movement into the field. Equivalently, forces driving nanoparticles find an equilibrium state where the magnetic force is balanced by the vector sum of the recoil forces. When only a magnetic force is present (recoil and pressure gradient forces are absent or neglected), direct integration of the magnetic force (Fm) gives $z(t) = \varepsilon(t) + z_0 \cos(4\pi f_m t)$ where $\varepsilon(t) = a_0 t^2$, and a_0, z_0 are constants and dependent on χ, V, B, and f_m is the modulation frequency of the magnetic flux density. The initial transient response of nanoparticles to the magnetic field (figure 6) contains both components of $z(t)$. As the low-pass filtered profile (figure 6(b) red line) indicates, the SPIO nanoparticles moved in one direction and soon movement was reduced. However, the Doppler frequency oscillation could be observed at the beginning of magnetic field application. In confined systems such as a microfluidic channel, $\varepsilon(t)$ becomes negligible at sufficiently long times (several seconds) because recoil and drag forces impede the free-space acceleration of the nanoparticles. Once forces on the nanoparticles equilibrate, free-space acceleration of the SPIO nanoparticles approaches zero and the sinusoidal variation of the magnetic force dominates nanoparticle displacement.

The nanoparticles used in our experiments are nanoscale while the probing beam had a wavelength of 1.3 μm so that individualized imaging is not possible. However, the data reported here represents an aggregate response to the probe beam. While it has been reported that the introduction of a magnetic field changes the amplitude of the fringe [8], we

applied the magnetic field in the same direction as the probing beam, so that phase changes of the nanoparticles, rather than the amplitude change, were produced and monitored. The minimum detectable concentration of nanoparticles was 0.21×10^{12} iron particles μl^{-1} (0.36 μg iron μl^{-1}) which is three times higher than the manufacture recommended dilution level (0.07×10^{12} iron particles μl^{-1}) for human procedures. The minimum detectable number of particles in the coherence volume, defined as beam spot area times coherence length of the MM-ODT, is 165×10^3. The sensitivity of the MM-ODT is about 90 dB, but by increasing the sensitivity of the system, one can expect to detect weaker concentrations. For example, a Fourier Domain OCT with 115 dB sensitivity may be able to detect 1500 particles per coherence volume. With increased sensitivity, spatial resolution can be increased by reducing the beam spot size and coherence length.

We have demonstrated the implementation of MM-ODT for superparamagnetic iron oxide nanoparticle imaging using an external oscillating magnetic field. Doppler shift leading to a phase modulation of the signal due to nanoparticle movement in the flow was introduced by applying a temporally oscillating high-strength magnetic field in the same direction as the probe beam. The controlled and increased Doppler frequency shift in MM-ODT with superparamagnetic nanoparticles may provide a new investigational tool to study superparamagnetic nanoparticle dynamics for nanosciences and various related studies.

Acknowledgments

This research was supported by research grants from the National Institutes of Health (AR47551, EB002495, EY01646201 and EB002021) and the Texas ATP.

References

[1] Artemov D 2003 Molecular magnetic resonance imaging with targeted contrast agents *J. Cell. Biochem.* **90** 518–24
[2] Fahlvik A K, Klaveness J and Stark D D 1993 Iron-oxides as Mr imaging contrast agents *J. Magn. Reson. Imaging* **3** 187–94
[3] Fercher A F, Drexler W, Hitzenberger C K and Lasser T 2003 Optical coherence tomography—principles and applications *Rep. Prog. Phys.* **66** 239–303
[4] Hartshorne H, Backhouse C J and Lee W E 2004 Ferrofluid-based microchip pump and valve *Sensors Actuators* B **99** 592–600
[5] Kim J, Oh J, Milner T E and Nelson J S 2006 Hemoglobin contrast in magnetomotive optical Doppler tomography *Opt. Lett.* **31** 778–80
[6] Oh J, Feldman M D, Kim J H, Condit C, Emelianov S and Milner T E 2006 Detection of magnetic nanoparticles in tissue using magnetomotive ultrasound *Nanotechnology* **17** 4183–90
[7] Oldenburg A L, Gunther J R and Boppart S A 2005 Imaging magnetically labeled cells with magnetomotive optical coherence tomography *Opt. Lett.* **30** 747–9
[8] Oldenburg A L, Toublan F J J, Suslick K S, Wei A and Boppart S A 2005 Magnetomotive contrast for *in vivo* optical coherence tomography *Opt. Express* **13** 6597–614
[9] Park B H, Pierce M C, Cense B and de Boer J F 2003 Real-time multi-functional optical coherence tomography *Opt. Express* **11** 782–93
[10] Park B H, Pierce M C, Cense B, Yun S H, Mujat M, Tearney G J, Bouma B E and de Boer J F 2005 Real-time fiber-based multi-functional spectral-domain optical coherence tomography at 1.3 μm *Opt. Express* **13** 3931–44
[11] Pierce M C, Park B H, Cense B and de Boer J F 2002 Simultaneous intensity, birefringence, and flow measurements with high-speed fiber-based optical coherence tomography *Opt. Lett.* **27** 1534–6
[12] Raj K, Moskowitz B and Casciari R 1995 Advances in ferrofluid technology *J. Magn. Magn. Mater.* **149** 174–80
[13] Wang X J, Milner T E and Nelson J S 1995 Characterization of fluid-flow velocity by optical Doppler tomography *Opt. Lett.* **20** 1337–9
[14] Wang Y X J, Hussain S M and Krestin G P 2001 Superparamagnetic iron oxide contrast agents: physicochemical characteristics and applications in MR imaging *Eur. Radiol.* **11** 2319–31
[15] Weissleder R, Bogdanov A, Neuwelt E A and Papisov M 1995 Long-circulating iron-oxides for Mr-imaging *Adv. Drug Delivery Rev.* **16** 321–34
[16] Yang V X D, Gordon M L, Qi B, Pekar J, Lo S, Seng-Yue E, Mok A, Wilson B C and Vitkin I A 2003 High speed, wide velocity dynamic range Doppler optical coherence tomography (Part I): system design, signal processing, and performance *Opt. Express* **11** 794–809
[17] Zahn M 2001 Magnetic fluid and nanoparticle applications to nanotechnology *J. Nanopart. Res.* **3** 73–8
[18] Zhao Y H, Chen Z P, Saxer C, Xiang S H, de Boer J F and Nelson J S 2000 Phase-resolved optical coherence tomography and optical Doppler tomography for imaging blood flow in human skin with fast scanning speed and high velocity sensitivity *Opt. Lett.* **25** 114–6